Nano-Structures & Nano-Objects 26 (2021) 100756

Contents lists available at ScienceDirect

Nano-Structures & Nano-Objects

journal homepage: www.elsevier.com/locate/nanoso

Design of π-conjugated flexible semiconductive 2D MOF and MOF derived CuO nano-spheres for solvent free C-X (S, O) hetero-coupling catalysis with enhanced conductivity

Maxcimilan Patra [a,1], Soumen Kumar Dubey [a,1], Bibhas Mondal [a], Kajal Gupta [a], Angshuman Ghosh [b], Subhankar Mandal [c], Satyajit Hazra [c], Ajit Kumar Meikap [d,*], Ujjal Kanti Roy [a,*], Subham Bhattacharjee [a,*], Rajat Saha [a,*]

[a] Department of Chemistry, Kazi Nazrul University, Asansol-713340, India
[b] TCG Lifescience, Block BN, Sector V, Saltlake, Kolkata-700156, India
[c] Saha Institute of Nuclear Physics, HBNI, 1/AF Bidhannagar, Kolkata 700064, India
[d] Department of Physics, NIT Durgapur, Durgapur-713209, India

ARTICLE INFO

Article history:
Received 1 January 2021
Received in revised form 15 April 2021
Accepted 28 April 2021

Keywords:
2D MOF
$\pi \cdots \pi$ Interaction
Flexible MOF
MOF derived CuO-NPs
Green catalysis
Electrical conductivity

ABSTRACT

A flexible, 2-fold interpenetrated 3D supramolecular structure $[Cu(ndc^{2-})(1,10\text{-phen})]_n$ (where ndc^{2-} = 2,6-napthalenedicarboxylate and 1,10-phen = 1,10-phenanthroline) comprising neutral 2D metal–organic layers as the basic building block was prepared. Structural study reveals that metal ions are bridged by ndc^{2-} ligands to form 2D coordination layers and the coordinated 1,10-phen moieties are hanging from the layers in the interlamellar spaces. The gliding motion of $\pi \cdots \pi$ stacked layers through 1,10-phen moieties was found to be responsible for the flexibility of MOF and the consequent extended conjugation also rendered semiconducting behaviour in the material. Thermal stability studies revealed that the framework was pretty stable below 260°C. Additionally, the MOF was characterized by performing BET adsorption and photoluminescence studies. Further, the MOF was calcinated at 650°C to prepare well defined, nearly uniform and spherical shaped CuO nanoparticles (CuO-NPs) with an average size of ~25 nm. Interestingly, CuO-NPs showed around 16 times more conductivity (4.8×10^{-2} S/cm) in relative to the parent MOF (3×10^{-3} S/cm). CuO-NPs induced cross-coupling reactions of alcohols and thiols with arylhalides have been reported. A simple, general, ligand-free and solvent-free procedure for the efficient synthesis of the cross-coupled products in high yield was successfully demonstrated.

1. Introduction

In last three decades, metal–organic frameworks (MOFs) are appeared as one of the most promising functional material due to their inherent porous structure and modular behaviour [1]. Initially, the inception was that the implication of inert metal ions and insulating bridging ligands makes MOFs weakly conducting or insulating in nature [2]. But, from last decade, design of conducting MOFs has gained much attention due to their several applications in energy storage, sensing, electrocatalysis, etc. [3]. Researchers have developed two different types of conductive MOFs: (a) intrinsically conductive MOFs: electrically conducting organic building blocks, such as 2,3-pyrazinedithiolate [4], dihydroxybenzoquinone [5] etc. have been used to induce conductivity in the designed framework, and (b) extrinsically conductive MOFs: electrically conducting guests, both neutral I_2, [6] (TCNQ) [7], and charged (BF_4^-) [8], are incorporated in the void space of MOFs to enhance conductivity. Intrinsically conducting MOFs have gained much attention over its extrinsic counterpart due to low cost production and easy synthesis [2a], [9]. Several types of design principles have been adopted by scientists to build intrinsically conducting MOFs: (a) use of metal ions and bridging ligands having equivalent band structure which will help to transport electrons through the framework [10], (b) use of radical generating ligands that will boost the conductivity of the designed framework [5c,10b] (c), use of extended $\pi \ldots \pi$ conjugation between 2D coordination polymer [5b], [11]. In organic electronics, π-interaction is used to develop conducting materials [12] and, in similar way, several research groups have developed conducting MOFs based on extended $\pi \ldots \pi$ conjugation using different

* Corresponding authors.
E-mail addresses: meikapnitd@yahoo.com (A.K. Meikap), uroccu@gmail.com (U.K. Roy), sbpb2012@gmail.com (S. Bhattacharjee), rajat.saha@knu.ac.in (R. Saha).

[1] Both have equal contributions.

https://doi.org/10.1016/j.nanoso.2021.100756
2352-507X/

organic ligands e.g. napthalenediimide, [9b] tetrathiofulvalene [13], anthracene [14], etc. Formation of continuous π-conjugation throughout the framework is the primary condition to design such materials. Herein, we have used 1,10-phen, highly potential to participate in $\pi \ldots \pi$ interaction, as the building block to develop conducting material and found that the synthesized 3D supramolecular framework showed semiconducting behaviour.

Recently, syntheses of various nano-materials using MOFs as sacrificial scaffolds are of great interest [15]. The regular periodic arrangement of metal nodes within the MOF architecture provides an excellent platform to design nano-particles of uniform size distribution as well as their intriguing porosity. The structure, composition, phase and size of the nano-particles can be controlled by optimizing the synthetic conditions: chemical environment (O_2, N_2 etc.), temperature and synthetic methods [16]. Several research groups have synthesized metal, [16a] metal–oxide, [16b,16c,16d,16e,16f,16g] mixed metal–oxide, [16h] metal carbide [16i] NPs, etc, and explored their enormous applications in gas adsorption, [16j] catalysis, [16b] and so on. Besides, these MOF derived NPs have been used for several types of electronic applications like electrocatalysis, [17] battery, [18] etc. based on their versatile conducting properties from insulating to metallic behaviour [17–19]. In this work, we have used our synthesized semiconductive MOF to develop NPs and interestingly found that the MOF-derived NPs showed higher conductivity than the parent MOF.

C–O and C–S bonds are prevalent in numerous compounds that are of biological, pharmaceutical, and material interest [20]. Specially, a large variety of aryl sulfides are in use for diverse clinical applications [21]. One of the most common synthetic methods for their preparation is the copper-assisted classic Ullmann reaction. However, these reactions often require harsh conditions such as high temperature (>200 °C), stoichiometrically higher amount of copper reagent and thus produce a lot of wastes [22]. Currently, to follow strict environmental laws, chemical based industries are desperate in reducing various harmful chemical wastes by designing intelligent catalysts those perform in mild or environment benign conditions with high yield, large selectivity and good efficacy [23]. Palladium and copper complexes containing electron-rich ligands have been studied considerably for the cross-couplings of oxygen and sulphur nucleophiles with aryl halides [24]. Subsequently, few studies have focused on the use of iron and nickel-based catalytic systems for this purpose also [25]. Unlike homogeneous catalyst, use of heterogeneous catalyst is much more advantageous in terms of their easy separation, recyclability, high thermal stability and longer lifetime. In this respect, we have focused on CuO-NPs induced heterogeneous C(aryl)-S and C(aryl)-O hetero-coupling reactions with the following advantages: (a) the reaction proceeds under solvent free condition, (b) easy separation of catalysts and products from the reaction mixture after completion, (c) high selectivity of the catalysts for the substrate, (d) high catalysis rate and e) re-usability.

In this endeavour, we have synthesized a 2-fold interpenetrated, flexible, 3D supramolecular framework: **[Cu(2,6-ndc)(1,10-phen)]$_n$**, by solvothermal method and characterized by SCXRD analysis. Structural analysis revealed that each Cu centres are connected by 2,6-ndc ligands to form 2D coordination layers with hanging coordinated 1,10-phen moieties and these 2D metal–organic coordination layers are assembled by 1,10-phen mediated $\pi \ldots \pi$ interactions to form the overall 3D supramolecular structure. The presence of $\pi \ldots \pi$ interactions help to: (i) induce flexibility and (ii) create electronic conducting pathway within the framework. The resultant flexible framework showed semiconducting nature in association with micro-porosity. TGA analysis revealed that the framework decomposes at 350 °C. The MOF was decomposed by heating at 650 °C to produce CuO-NPs which were characterized by PXRD, SEM and EDAX analyses. Four probe electrical conductivity experiments revealed that the synthesized CuO-NPs have 16 times higher conductivity than parent MOF. Further, we have successfully demonstrated solvent free C–S and C–O heterocouplings in excellent yields in bulk utilizing the CuO-NPs. Product analysis revealed exclusive formation of the desired products with minimum amounts of wastes; hence, we would be able to make the process green and highly applicable for industrial scale synthesis.

2. Experimental section

Materials and Methods: Copper (II) nitrate, monohydrate; 2,6-napthalene dicarboxylic acid and 1,10-phenanthroline were purchased from Merck chemical company. All other chemicals used were AR grade. Elemental analysis (C, H, N) was carried out using a Perkin-Elmer 240C elemental analyzer. The thermal analysis was carried out using a Mettler Toledo TG-DTA 85 thermal analyzer under a flow of N_2 (30 ml/min). The sample was heated at a rate of 10 °C/min with inert alumina as a reference. IR spectroscopy was measured on Nicolet Impact 410 spectrometer between 400 and 4000 cm^{-1}, using the KBr pellet method. Photoluminescence spectra were collected on a Shimadzu RF-5301PC spectrophotometer. Powder XRD patterns were recorded by using Cu-Kα radiation (Bruker D8; 40 kV, 40 mA). The elemental analysis for CuO-NPs was performed by BRUKER energy dispersive X-ray spectrometer (EDS) attached with the FEI, INSPECT F50 field emission scanning electron microscope (FESEM). ^{1}H-NMR studies were carried out by using 300 MHz Bruker NMR spectrometer. The XPS measurements of the sample was carried out in an ultrahigh vacuum (UHV) multiprobe setup (Omicron Nanotechnology) at a base pressure of $\sim 2.0 \times 10^{-9}$ mbar, which was equipped with an EA125 hemispherical energy analyzer and an X-ray source [26]. For the XPS measurements, monochromatic Al Kα X-ray of 1486.6 eV photon energy was used as a source and the corresponding spectrometer energy resolution was $\sim$ 0.8 eV. C 1s level (binding energy of 284.8 eV) was chosen as the reference level to calibrate the other core-level spectra.

Synthesis of Complex 1 {[Cu(O-phen)(ndc)]$_n$: A mixture of $Cu(NO_3)_2$ (0.5 mmol, 0.1214 g), ndc (0.5 mmol, 0.1092 g), 1,10-phen (0.25 mmol, 0.0502 g) and 1 mL Et_3N in 6 mL DMF was stirred for 15 min. Then the mixture was transferred into a 15 ml Teflon-lined stainless-steel vessel and heated for 24 h at 120 °C. Afterwards, it was cooled to room temperature for another 24 h. After 48 h, green coloured single crystals (Figure S1) suitable for X-ray structure determination were isolated by filtration. Yield: 70%. Anal. Calcd. for $C_{24}H_{14}CuN_2O_4$ indicates C: 62.85% (62.88% theo), H: 3.10% (3.12% theo) and N: 6.10 (6.08% theo). IR (KBr pellet, cm^{-1}): 1606(s), 1560(s), 1544(w), 1426(w), 1394(s), 1357(s), 1221(w) and 1191(w) (Figure S2).

Electrical conductivity measurement: The resistance of the sample is measured by means of a four terminal direct current technique with resolution of $\delta R/R = 10^{-5}$ using a pressed pellet (10 ton pressure) of the samples. The four terminal connections are made using fine copper wire with pure silver paste. As a confirmatory test towards ensuring good electrical contact using silver paste, the continuity of the samples was checked before placing it within the sample holder. Contribution of conductivity of silver of the paste is ignored as it is used for all cases. All these measurements were performed by the following equipments, (i) A constant current source (KEITHLEY INSTRUMENT, Model 220), (ii) A nanovoltmeter (KEITHLEY INSTRUMENT, Model 181), (iii) Hewlett Packard 3458 A, 81/2 digit multi-metre.

General Procedure for C-X (X = S and O) Hetero-coupling Reactions: The catalytic reactions were carried out in a glass batch reactor. To a stirred solution of the phenol or thiophenol

(25 mmol), aryl halide (5 mmol), KOH (5 mmol) and CuO (2.5 mol%) were added, and the reaction mixture was stirred at 100 °C for 17 h under inert atmosphere and monitored continuously by TLC (hexane/ethyl acetate = 9:1 v/v). After completion of the C–O or C–S cross-coupling of phenol/thiophenol with aryl halide, (i.e. after complete consumption of the aryl iodide which takes near about 17 h), the reaction mixture was treated with diethyl ether. The solution was centrifuged and then catalyst was isolated, washed water and ether. After complete drying, the catalyst can be reused for the next cycle. The remaining mixture was diluted with water and extracted with diethyl ether thrice. The combined organic layer was dried over anhydrous Na_2SO_4, filtered, and concentrated to afford the crude material. The crude material was then purified by column chromatography (silica 100–200 mesh, ethyl acetate-hexane 5%–10%) to afford the desired C–O or C–S cross coupling product (yield = 95%–99%).

Crystallographic Data Collection and Refinement: Suitable single crystal of the complex was mounted on a Bruker SMART diffractometer equipped with a graphite monochromator and Mo-K_α(λ = 0.71073 Å) radiation. Unit cell parameters were determined by using the APEX2 [27] program. Data reduction was carried out by the SAINT [27] program and correction or absorption was performed using the SADABS [27] program. The structure was solved using Patterson method by using the SHELXS-2018/3 [28] embedded in WINGX software package [29]. Subsequent difference Fourier synthesis and least-square refinement revealed the positions of the remaining non hydrogen atoms. Non-hydrogen atoms were refined with independent anisotropic displacement parameters. Hydrogen atoms were placed in idealized positions and their displacement parameters were fixed to be 1.2 times larger than those of the attached non-hydrogen atom. All Figures were drawn by using PLATON [30] and ORTEP [31]. Data collection and structure refinement parameters and crystallographic data for complex 1 are given in Table S1. The structure was previously reported in literature [32] and, herein, we have described from a different perspective. Some selected coordination bond lengths, bond angles and non-covalent interaction parameters are summarized in Table S2-S3.

Indexing of the PXRD data: The indexing of the XRPD pattern was carried out using NTREOR and McMaille programs of EXPO 2009. Indexing reveals that the complex is still crystalline with a monoclinic system with a = 13.5426 Å, b = 13.9326 Å, c = 12.0862 Å, β = 100.1023° and V = 2245.11 Å^3. The space group was obtained from statistical analysis of the powder pattern with the help of find space module of the EXPO 2009 software package. Statistical analysis shows that the most probable space group is $P2_1/n$. For this unit cell and space group, full pattern decompositions were performed using Le Bail method giving good fit between calculated and experimental powder X-ray patterns. This result was corroborated from the indexing and Pawley refinement of the PXRD pattern of the complex by the reflex module of the Material studio program. Unit cell, peak profiles, zero-shift, background were refined simultaneously. Peak profiles were refined by the Pseudo-Voight function with Berar–Baldinozzi asymmetry correction parameters. The background was refined using a 4th order polynomial.

3. Result and discussions

Structural description of Complex 1: X-ray crystal structure analysis revealed **1** as a neutral 3D supramolecular framework (formula $[C_{24}H_{14}CuN_2O_4]_n$). The asymmetric unit contains one Cu(II) ion, two halves two ndc^{2-} ligands and one 1,10-phen (Figure S3). Each Cu(II) atom shows distorted square pyramidal geometry (τ = 0·07) with CuN_2O_3 chromophore (Figure S4). ndc^{2-} ligands show two different types of bridging modes: μ4-*bis*-bridging and μ2-*bis*-bridging. Coordination of two different types of ndc^{2-} with the Cu^{2+} ions forms 2D coordination sheet in the ***bc***-plane with 1,10-phen ligands hanging into the interlamellar spaces from the metal centres, Figure S5. These 1,10-phen moieties between two 2D layers are connected through are interacted by $\pi \ldots \pi$ interactions between aromatic rings present within the 1,10-phen molecules. Such $\pi \ldots \pi$ interactions further assemble these 2D layers along *a*-axis to generate a spongy 3D supramolecular framework, as shown in Fig. 1a. The dimensions of all $\pi \ldots \pi$ interactions are listed in Table S4. It is to be noted that 1D channel of dimension 12.071 × 13.294 Å is formed along ***a***-axis (Figure S6). The channel is filled by two-fold self impregnation in order to achieve an efficient packing (Fig. 1b and S7).

Framework Stability and PXRD: Thermo-gravimetric analysis of the compound was performed in the temperature range of 25–500 °C under N_2 atmosphere (Fig. 2). The TG analysis indicated that complex **1** is stable up to 260 °C and undergoes decomposition in two consecutive steps above this temperature. In the first step, 1,10-phen moieties undergo dissociation within 260 and 300 °C and above this temperature it degrades in another step at about ∼325 °C.

To know about framework flexibility, the PXRD analyses with complex **1** were done at room temperature and at 150 °C temperature. The PXRD pattern of the as synthesized complex **1** is matched very well with the simulated pattern which indicated the phase purity of the sample. The PXRD (Fig. 3) pattern at higher temperature has peaks at slightly lower angle. The indexing of the PXRD pattern was carried out using NTREOR and McMaille programs of EXPO 2009 (supporting information, Figure S8). This reveals that the complex is still crystalline with monoclinic system (***a*** = 13.5426, ***b*** = 13.9326, ***c*** = 12.0862 Å, ***β*** = 100.1073° with a larger cell volume of 2245.11 Å^3, Table S4). So, the length of the ***a***-axis, along which 2D layers are stacked through $\pi \ldots \pi$ interactions, increases in large amount compared to ***b***- and ***c***-axes and this corresponds to the expansion of layer gap assisted by the gliding motion of the π-stacked layers [33], which is feasible for 1,10-phen ligand. So, both the increase in bond length and expansion of layer gap along ***a***-axis contribute to the overall 15% increase in the overall cell volume. Upon cooling to room temperature, the PXRD pattern reverts back to the original pattern. This proves the π-induced flexibility of the framework.

Adsorption study: Though PLATON study indicates the non-porous nature the framework at ambient condition but the variable temperature PXRD study showed that there is a chance to create porous channel along crystallographic ***c***-axis by thermally stimulated π-induced flexibility — and thus we have attempted to analyse sorption behaviour of the sample. N_2 adsorption study at 77 K revealed the non-porosity of the material while the solvent sorption studies at 298 K indicated micro-porosity. Water adsorption isotherm (at 298 K) of complex showed type **III** behaviour. The volume uptake of water is 15.6 cm^3/g (Fig. 4). Complex **1** also adsorbs 12.9 cm^3/g methanol and 6.24 cm^3/g ethanol (Fig. 4). Small amount of adsorption may be interpreted as that due to interpenetration very narrow channels were created within the framework or surface adsorption [34]. Desorption curve does not coincide with the adsorption curve in all cases, showing a hysteresis loop and incomplete desorption. A very little amount of water, methanol and ethanol remains within the framework. Small hysteresis in the water adsorption isotherm is probably because of trapping by the coordinatively unsaturated metal sites.

Photoluminescence: Photoluminescence property of complex **1** was performed at room temperature in solid state. The emission spectra of both 1,10-phen ligand and complex **1** are shown in

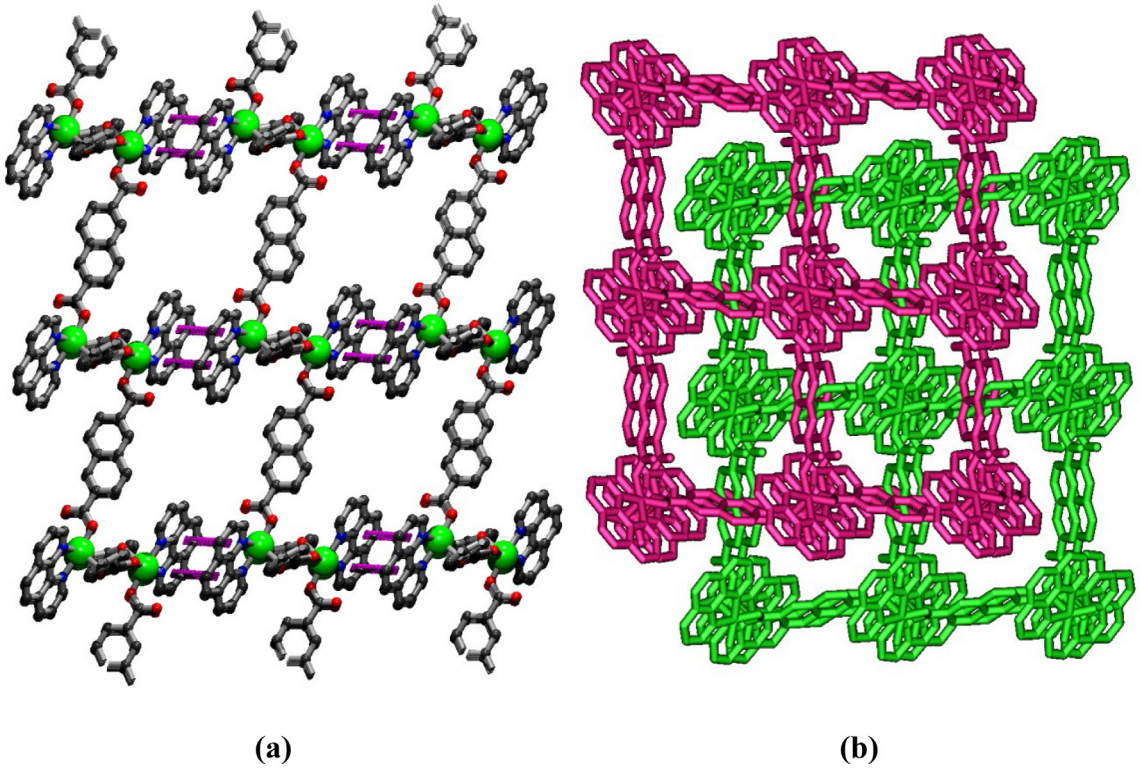

Fig. 1. $\pi \ldots \pi$ (magenta) conjugated 3D supramolecular structure (a) and 2-fold interpenetration (b) of complex **1**. (For interpretation of the references to colour in this figure legend, the reader is referred to the web version of this article.)

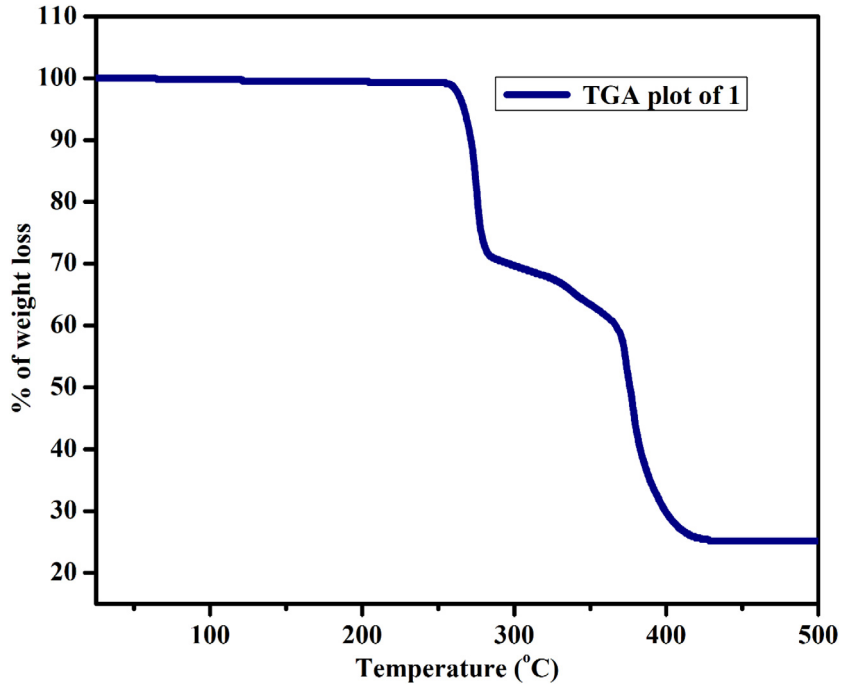

Fig. 2. The thermal plot of complex **1**.

Figure S9. The luminescence spectra of 1,10-phen ligand show two peaks at 412 nm and 434 nm with a shoulder at 461 nm. The spectra arise due to π-π^* transition. The luminescence spectra of complex 1 show similar pattern — the spectra contain two peaks at 414 nm and 434 nm with three different shoulders at 458 nm, 464 nm and 468 nm. The spectra arise due to both intra-ligand π-π^* transition and M-L charge transfer transition. So due to metal complex formation, a small red shift occurs.

Synthesis and Characterization of CuO-NPs: Nano-particles are highly interesting as their properties are critically dependent on synthetic condition, size distribution, morphology and shape.

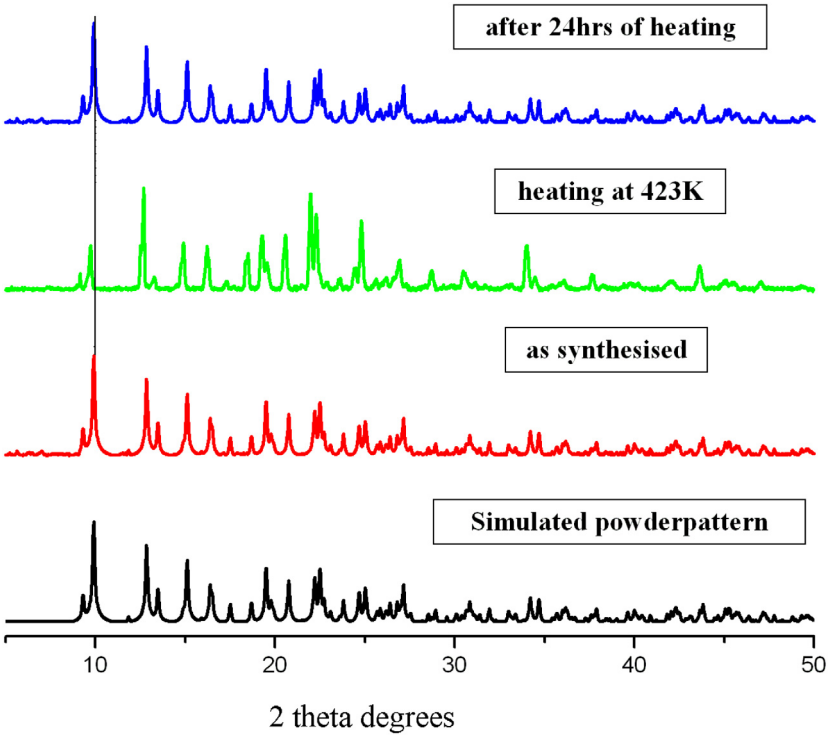

Fig. 3. Variable temperature PXRD pattern of **complex 1**.

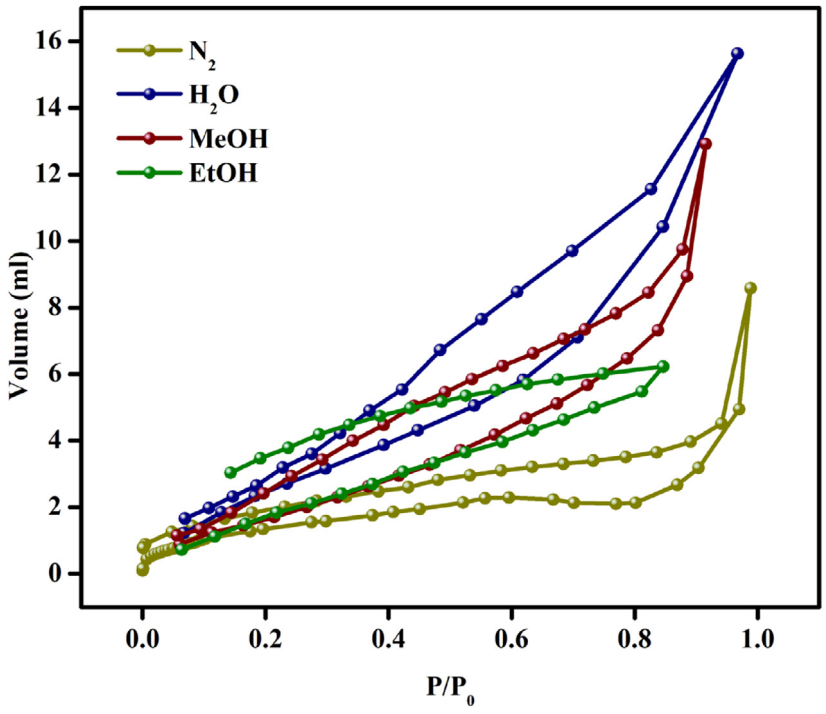

Fig. 4. Gas and solvent sorption behaviour of complex **1**.

CuO-NPs have great potential for their applications in electrochemical cells, magnetic storage media, photovoltaic cells, etc. Here, the 2D-MOF is used as a template to synthesize CuO-NPs by calcinations. The bulk material of the MOF was heated at 650 °C for 4 h at normal condition. Upon heating, the green coloured compound turned in black powder, which was characterized by PXRD, EDS, IR, TEM and SEM analyses. IR spectra of the CuO-Nps are presented in Figure S10. The PXRD pattern matches with the reported PXRD pattern of CuO with JCPDS No. 08-0234 (Fig. 5a). The TEM micrograph indicated the spherical morphology of the synthesized NPs (Fig. 5b) with average size of ~25 nm and this corroborates with the PXRD data. EDS study indicated the presence of characteristic peaks for the constituents (Cu and O) (Figure S11). The Cu $2p_{3/2}$ core-level spectra (Fig. 6) have been studied to know the oxidation state of Cu present in the copper oxide nanoparticles. The binding energy position of the

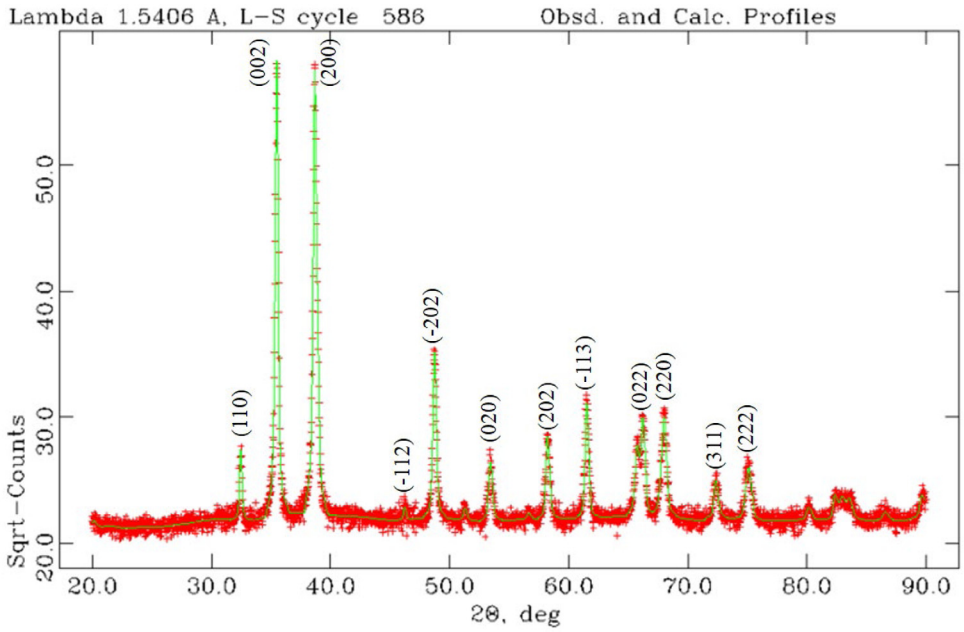

(a)

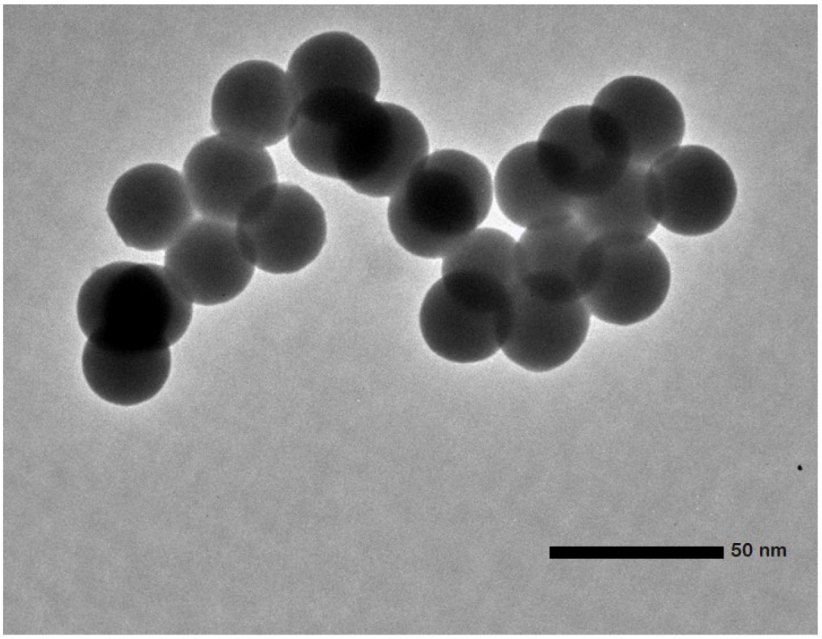

(b)

Fig. 5. PXRD pattern (a) and TEM image (b) of the synthesized CuO-NPs.

main peak in the spectra was observed at around 933.7 eV that informs about the presence of Cu^{2+} species, which was observed previously by many people [35]. The strong shake-up satellite observed in these spectra is also an indication of the presence of Cu^{2+} species that was mentioned by many authors previously [35]. So, the Cu $2p_{3/2}$ core-level spectra confirm that the Cu present in this copper nanoparticles sample is mostly in the Cu^{2+} oxidation state.

Green Catalytic C-X Hetero-coupling Reactions: In the present work, the synthesized spherical shaped CuO-NPs are used for the catalytic cross-coupling (C–O and C–S) reactions of alcohols and thiols with arylhalides. Generally, for such C–O and C–S cross-coupling reactions, high boiling solvents like DMSO, DMF, NMP, etc. are required in both homogeneous and heterogeneous conditions. And consequently, separation of products from these solvents becomes very difficult and tedious. Here, we are going to report a solvent free, neat reaction protocol for such hetero-coupling reactions of phenol, thiophenol, alcohol, and thiols with aryl halides.

Literature review indicates that in previous studies of copper-catalyzed hetero-coupling reactions, *N*-methylpyrrolidinone (NMP), dimethylformamide (DMF), dimethylsulfoxide (DMSO)

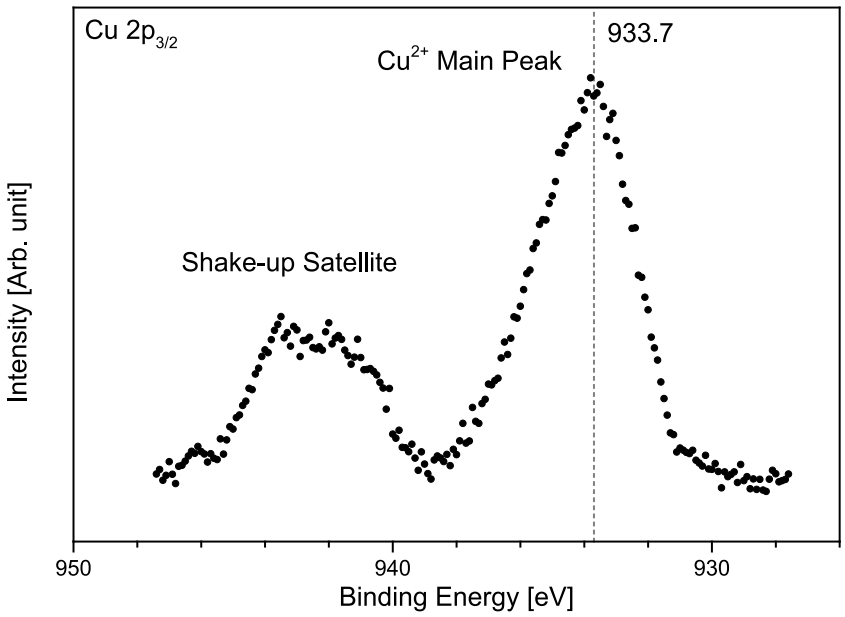

Fig. 6. XPS data of CuO-NPs reveals the presence of only Cu^{2+} ions.

etc. are used as solvent with KOH and K_2CO_3 as base [36] and, thus here, we have also followed the same protocol initially. Punniyamurthi et al. have carried out the C-X (X = S, N and O) hetero-coupling catalytic reactions using CuO-NPs in DMSO [36d]. Here, catalytic activity of the synthesized CuO-NPs was first investigated for the cross-coupling of iodobenzene with phenol and latter with thiophenol. The reactions of chlorobenzene, bromobenzene, phenyltosylate, and phenylboronic acid are studied, but those are found to be inferior to that of aryl iodides. Catalytic tests were also performed with CuCl, CuBr and CuI, freshly prepared before use, provided the same results as obtained with synthesized CuO-NPs. Other Cu(II) salts tested ($CuBr_2$, $CuSO_4 \cdot 5H_2O$, $CuCl_2$) were found to be less efficient catalysts (yields 55%–69%) than the CuO-NPs. A low amount of 2.5 mol % of CuO-NPs was employed in these initial standardization reactions. Our first goal was to optimize reaction conditions and to achieve information about the role of additives and solvent polarity. It appeared that, by applying KOH as base in DMF, diphenylether was obtained in quantitative yield in presence of 20 mol% CuO-NPs catalyst without the use of added ligands. Solvent polarity has significant impact on the yield of the reactions (Table S5) – high polarity solvents like DMF, DMA and NMP show better yield than toluene (entries 3–5). It is noteworthy that very low yield (40%) was obtained for using water as solvent (Table S5, entry 6). Now, difficulty in separation of these solvents from the product prompted us to choose the neat reaction conditions (Table S5, entry 7). And interestingly, we have found that the yield of neat reaction conditions are similar to that in DMF, DMA and NMP and then we decided to go further with the neat reaction conditions.

Similarly, a series of bases were also screened. Among inorganic bases, KOH gave almost quantitative results for the coupling reaction to diphenylethers (Table S6), while, among organic bases, triethylamine and Hunig's base (DIPEA) gave also good results (Table S6, entries 2 and 3) in heterogeneous reaction mixture. Notably, in our case the required amount for the base is only one equiv. (based on the aryl halide), while in common reports this is usually in between 1.5 and 2.5 equiv. Further experiments were performed to find the optimal reaction temperature and reaction time. Both Tables S5 and S6 refer to around 17 h reaction with temperature of 100 °C. It was noted that a small decrease in temperature of only 10 °C caused a significant decrease in diaryl thioether yield (85%). Lowering the time of the reaction in the present conditions also decreases the yield of the desired products. Accordingly, at 100 °C, the reaction of iodobenzene with phenol is relatively fast (65 and 95% after 2 and 6 h, respectively). It also appeared that fluoro-, chloro-, and bromobenzene are very less reactive under the optimized conditions, giving extremely lower yields (4%–55%) of the C–O coupling products (Table S7). Aryltosylate and boronic acids are also very less effective compared to that of iodide (Table S7, entries 5 & 6). Finally, the effect of the copper catalyst and its loading amount was evaluated. As discussed earlier and shown in Table S8, Cu(II) catalysts performed badly (Table S8, entries 1–4, yields 55%–69%). Only a minor difference in yields were observed when catalytic activity of CuO-NPs was compared with Cu(I) salts (Table S8, entries 5–8). The desired products are purified by column chromatography, identified by NMR spectra and then the isolated yield was calculated.

Table 1
Reaction of Aryl Iodides with Phenol and Thiophenol (conditions: phenol or thiophenol (25 mmol), aryl iodide (5 mmol), KOH (5 mmol), CuO (2.5 mol%), 100 °C, 17 h.

Entry	Aryl iodide	Alcohol or thiol	Product	Yield (%)
1	PhI	PhOH	Ph-O-Ph	99
2	PhI	PhSH	Ph-S-Ph	99
3	PhI	$PhCH_2OH$	$PhCH_2$-O-Ph	95
4	PhI	$PhCH_2SH$	$PhCH_2$-S-Ph	95

To determine the scope of the catalytic system, the present protocol was further applied to reactions of a variety of commercially available aryl iodides and phenols or thiophenols (Table 1). As shown in Table 1, the coupling of phenol and thiophenol with iodobenzene was successful, leading to the desired products in good yields. The protocol is equally efficient for aromatic and aliphatic phenols and thiophenols. The catalyst system is highly efficient providing the corresponding diaryl ethers and thioethers in good to excellent yields. Iodobenzene was maintained as arylating substrate. The present optimized catalytic process provides the arylation of phenols and thiophenols with aryl iodides, in the presence of KOH as a base under neat conditions. To the best of our knowledge, this is the first report about aryl-sulphur and aryl-oxygen bond formation in which a MOF derived CuO-NPs catalyst

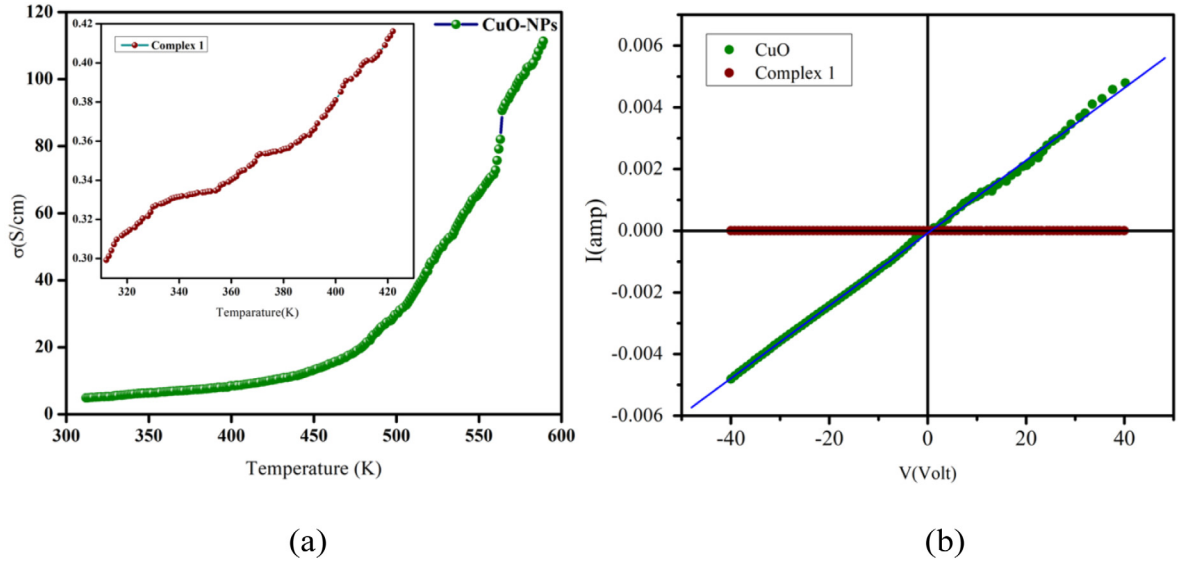

Fig. 7. Variable temperature electrical conductivity and corresponding I–V curve of the both complex **1** and MOF derived NPs.

is used without addition of any ligand and solvent. In the present study diphenylether and diphenylthioether was formed in 99% yield in the reaction of iodobenzene with phenol and thiophenol in solvent free neat conditions.

The CuO nanoparticles are recyclable upto 5th cycle without loss of significant reactivity (Table S9). After completion of the C–O cross-coupling of phenol with iodobenzene, the reaction mixture was treated with diethyl ether. Then, the overall mixture was centrifuged to isolate the catalyst. After isolation, it was washed with water and ether repeatedly and then dried for further use (Figure S13). The reusability tests indicate high yield. A comparative study with the bulk CuO synthesized by precipitation method was also studied – a lower amount of yield (∼40%–55%) was obtained for CuO bulk.

The catalytic activity of our synthesized CuO-NPs was investigated for the cross-coupling of iodobenzene with phenol and compared with similar heterogeneous catalysts (Table S10). Unlike homogeneous catalyst, use of heterogeneous catalyst is much more advantageous in terms of their easy separation, recyclability, high thermal stability and longer lifetime. In this respect, based on literature and availability of the heterogeneous catalysts, the reactivity of ZnO, SnO, SnO_2, CuO, Cu_2O and CuO NPs/SiO_2 [37] has been judged and compared with respect to C–O coupling reaction of phenol and iodobenzene. Our synthesized CuO is found to be most effective with respect to yield of the desired coupling product. Heterogeneous catalysts other than CuO and Cu_2O found to be completely ineffective giving no yield of the desired C–O coupling product (entries 1–3).

A suitable mechanistic pathway for the above-mentioned catalysis reactions was proposed (Scheme S1). These results suggest that the reaction may occur by oxidative addition followed by reductive elimination. The oxidative addition of the aryl halide with catalyst can give intermediate **A**, which can undergo reaction with an alcohol or thiol to afford intermediate **B**. Intermediate **B** can provide the C–O or C–S cross coupling product by reductive elimination. According to Sambiagio et al. the mechanism of such reactions is still unclear and it is considered that the mechanism actually varies depending on the substrate, ligand and reaction conditions [22b]. It is believed that the most active catalyst is Cu(I)-species which may form from the initial copper source.

Electrical Conductivity of MOF and MOF derived CuO-NPs: In complex **1**, the coordination between the metal centres and ndc^{2-} ligands forms 2D coordination layers and coordinated 1,10-phen moieties are hanging from the layers to connect next to neighbouring layers through $\pi \ldots \pi$ interaction to form 3D supramolecular structure. Due to the presence of extended $\pi \ldots \pi$ conjugation within the structure of **1**, we hope that the framework may show electrical conductivity. Bulk electrical conductivity of complex **1** has been measured by four probe contact using Ag wire on the pressed pellets. The conductivity of complex **1** is 3 x 10^{-3} S/cm at 312 K with Ohomic behaviour within the range of ± 40 V, Fig. 7(a and b). Variable temperature conductivity measurement within the temperature range of 312 K to 423 K indicates that with increasing temperature, conductivity of the framework increases — the framework is semiconducting in nature. The conductivity value is 4.2 × 10^{-3} S/cm at 423 K. With increasing temperature, delocalization of π-electrons increases and this may be a reason behind the linear rise in conductivity value electrical conductivity. The calculated activation energy of the framework is 0.077 eV.

Koo et al. have reported a semiconductive metal–organic framework having 2,5,8-tri(4-pyridyl)1,3-diazaphenalene as the π-conjugated ligand. Single crystal electrical conductivity measurement gives a value of ∼1 x 10^{-6} S/cm [12a]. Kuang et al. have reported single crystal conductivity value of ∼1.2 × 10^{-5} S/cm of a framework having napthalenediimide [12b]. Haider et al. have measured conductivity on the single crystal of a framework containing 1,4,5,8-naphthalenetetracarboxylate and the framework shows conductivity of ∼10^{-4} S/cm [12c]. Chen et al. have reported the semiconducting behaviour of mixed metal MOF in which 4,4′-(anthracene-9,10-diylbis(ethyne-2,1-diyl))dibenzoate is used to induce $\pi \ldots \pi$ interaction within the framework at separation distance of 3.4 Å [12d]. Electrical conductivity measurement on single crystals gives a conductivity value of 1.3 × 10^{-3} S/cm. Qu et al. have measured electrical conductivity of a metal–organic framework containing N,N′-di(4-pyridyl)-1,4,5,8-naphthalenetetracarbox-diimide on both single crystal and pressed pellets [12e]. Single crystal conductivity measurement showed 10^3 times higher conductivity (3.3 × 10^{-3} S/cm) than measured on the pressed pellets (7.6 × 10^{-6} S/cm). In our case, four probe electrical conductivity measurement on the pressed pellet of complex **1** gives a value of 3 x 10^{-3} S/cm at 312 K.

We have also studied the electrical conductivity of the MOF derived CuO-NPs in a similar manner. CuO is a p-type semiconductor but the bandgap and electrical conductivity vary with

the size and morphology of the nano-particles [38]. In most cases, the bandgap of CuO-NPs varies in the range of 1.2 to 2.0 eV and, based on its narrow bandgap, CuO-NPs have significant applications in electronic and opto-electronics. The conductivity of the MOF derived CuO-NPs is 4.85 $\times$ 10^{-2} S/cm with similar Ohomic behaviour at 312 K and this conductivity value is 16 times higher than the parent MOF, Fig. 7a and b. Combustion of the organic moieties within the MOF leads to the occurrence of charge transfer interaction between the copper and oxygen atoms within the framework and this may be the reason behind this enhanced conductivity. The variable temperature conductivity of the NPs is measured within the range of 312 to 588 K and the CuO-NPs also show semiconducting behaviour. The conductivity value rises smoothly up to 430 K (11 x 10^{-2} S/cm) and afterwards increases very rapidly to 1.11 S/cm at 588 K. A plot of $\ln(\sigma)$ vs. 1000/T for CuO-NPs shows two linear portions intersecting each other (Figure S14). This indicates the presence of two activation energy of CuO and values are 73 and 370 meV respectively, with a crossover at 430 K. The comparatively small activation energy indicates that Cu(I) and Cu(0) in association with oxygen vacancies may be present in CuO-Nps [16a]. Change of activation energy with temperature may be due to the presence of any metastable state in the sample.

4. Conclusions

Single crystal X-ray analysis of complex 1 revealed two types of binding modes (μ2- and μ4-) of ndc^{2-} ligands to the central Cu(II) ions, which, in turn, resulted in the formation of 2D coordination sheet. While the hanging 1,10-phenanthroline ligands in the interlamellar space assembled together by π-π interactions, which led to the formation of spongy 3D supramolecular metal–organic framework (MOF). Careful analysis of the MOF, which was stable up to 260 °C, depicted the presence of interpenetrated network topology. Reversible structural transformation of the framework by gliding motion of π-π stacked 1,10-phenanthroline ligands along the crystallographic *a*-axis and hence reversible expansion and contraction among the layer gap of 2D coordination sheets was confirmed by variable temperature PXRD measurements. Adsorption studies of the MOF with water, methanol and ethanol depicted a hysteresis loop in adsorption/desorption cycle. After thorough characterization of the MOF, it was calcinated at 650 °C for 4 h to fabricate CuO-NPs. The PXRD patterns confirmed the formation of CuO-NPs. While microscopic images showed formation of nearly uniform CuO-NPs with an average size of ~25 nm. Electrical conductivity measurements of the MOF and MOF derived CuO-NPs suggested both of them are semiconducting nature. However, CuO-NPs were found to be far more conducting compared to the parent MOF. Further, selective and efficient CuO-NPs catalyzed C–O and C–S bond-forming reaction of aryl iodides and various thiophenols is developed. This catalytic procedure offers general applicability and simplicity, avoiding the expensive and time-consuming preparation of suitable ligands and activated substrates. Based on controlled experiments and green chemistry rules, we proposed a solvent free, neat reaction conditions. Because of these advantages, we strongly believe that the protocol demonstrated in this work could find large application. And, we hope that such MOF derived nano-particle synthesis technique may be used for the synthesis of different types of metal–oxide nano-materials like ZnO, Cr_2O_3, VO_2, rare earth oxides.

CRediT authorship contribution statement

Maxcimilan Patra: Synthesized the materials and carried out most of the experiments, Writing manuscript. **Soumen Kumar Dubey:** Synthesized the materials and carried out most of the experiments, Writing manuscript. **Bibhas Mondal:** Carried out all the catalysis experiments, Written the manuscript. **Kajal Gupta:** Carried out all the electrical conductivity measurements, Written the manuscript. **Angshuman Ghosh:** Carried out several characterizations like NMR, IR, Manuscript preparation. **Subhankar Mandal:** Carried out the XPS measurement, Manuscript preparation. **Satyajit Hazra:** Carried out the XPS measurement, Manuscript preparation. **Ajit Kumar Meikap:** Carried out all the electrical conductivity measurements, Written the manuscript. **Ujjal Kanti Roy:** Carried out all the catalysis experiments, Written the manuscript. **Subham Bhattacharjee:** Idea of this research project was drawn, Manuscript preparation. **Rajat Saha:** Idea of this research project was drawn, Manuscript preparation.

Declaration of competing interest

The authors declare that they have no known competing financial interests or personal relationships that could have appeared to influence the work reported in this paper.

Acknowledgements

This work was supported by funding from TARE, SERB to R. S. (TAR/2018/000744) and DST Inspire Faculty Research Grant to S.B. (Faculty Registration No.: IFA18-CH304, DST/INSPIRE/04/2018/000329). U.K.R. acknowledges financial support of this work by SERB New Delhi, SR/FT/CS-137/2011 dated 12.07.2012, and Science and Technology and Biotechnology-WB, 50 (Sanc.)/ST/P/S&T/15G-10/2018 dated 30.01.2019 to UKR is gratefully acknowledged. M. P. and S. K. D. thank DST Inspire Faculty Research Grant for financial assistance. The authors thank Goutam Sarkar for his technical support in XPS measurements. S. M. acknowledges the Council of Scientific & Industrial Research (CSIR), India for providing a research fellowship.

Appendix A. Supplementary data

Supplementary material related to this article can be found online at https://doi.org/10.1016/j.nanoso.2021.100756. The CCDC number is 2013885 for complex 1. Figure S1–S9, Table S1–S8, NMR spectra and catalytic mechanism scheme are given in Supporting information file.

References

[1] (a) H. Furukawa, K.E. Cordova, M. O'Keeffe, O.M. Yaghi, The chemistry and applications of metal-organic frameworks, Science 341 (2013) 1230444.
(b) R. Chakraborty, P.S. Mukherjee, P.J. Stang, Supramolecular coordination: self-assembly of finite two- and three-dimensional ensembles, Chem. Rev. 111 (2011) 6810.
(c) T.K. Maji, R. Matsuda, S. Kitagawa, A flexible interpenetrating coordination framework with a bimodal porous functionality, Nat. Mater. 6 (2007) 142.
(d) J.A. Mason, M. Veenstra, J.R. Long, Evaluating metal-organic frameworks for natural gas storage, Chem. Sci. 5 (2014) 32.
(e) J.-R. Li, R.J. Kuppler, H.-C. Zhou, Selective gas adsorption and separation in metal-organic frameworks, Chem. Soc. Rev. 38 (2009) 1477.
(f) A. Corma, H. García, F.X.L. Xamena, Engineering metal organic frameworks for heterogeneous catalysis, Chem. Rev. 110 (2010) 4606.
(g) J.L.C. Rowsell, O.M. Yaghi, Metal-organic frameworks: a new class of porous materials, Microporous Mesoporous Mater. 73 (2004) 3.
(h) S. Kitagawa, R. Kitaura, S. Noro, Functional porous coordination polymers, Angew. Chem. Int. Ed. 43 (2004) 2334.

(i) W.P. Lustig, S. Mukherjee, N.D. Rudd, A.V. Desai, J. Li, S.K. Ghosh, Metal–organic frameworks: functional luminescent and photonic materials for sensing applications, Chem. Soc. Rev. 46 (2017) 3242.
(j) A.M. Al-Enizi, J. Ahmed, M. Ubaidullah, S.F. Shaikh, T. Ahamad, M. Naushad, G. Zheng, Utilization of waste polyethylene terephthalate bottles to develop metal–organic frameworks for energy applications: A clean and feasible approach, J. Clean. Prod. 248 (2020) 119251.
(k) A.M. Al-Enizi, M. Ubaidullah, J. Ahmed, T. Ahamad, T. Ahmad, S.F. Shaikh, M. Naushad, Synthesis of niox@ npc composite for high-performance supercapacitor via waste pet plastic-derived ni-mof, Compos. B. Eng. 183 (2020) 107655.
(l) M. Ubaidullah, J. Ahmed, T. Ahamad, S.F. Shaikh, S.M. Alshehri, A.M. Al-Enizi, Hydrothermal synthesis of novel nickel oxide@ nitrogenous mesoporous carbon nanocomposite using costless smoked cigarette filter for high performance supercapacitor, Mater. Lett. 266 (2020) 127492.
(m) N. Bakhtiari, S. Azizian, S.M. Alshehri, N.L. Torad, V. Malgras, Y. Yamauchi, Study on adsorption of copper ion from aqueous solution by mof-derived nanoporous carbon, Microporous Mesoporous Mater. 217 (2015) 173–177.
(n) H. Zhang, M. Zhang, M.V. Lin Ping, J. Tang, S.M. Alshehri, Y. Yusuke, D. Shaowu, J. Zhang, A highly energetic n-rich metal-organic framework as a new high-energy-density, Material. Chem. Eur. J. 22 (2015) 1141–1145.

[2] (a) N. Nidamanuri, K. Maity, S. Saha, Electrically conductive metal-organic frameworks, in: Book Chapter, World Scientific Publishing, 2017.
(b) V. Stavila, A.A. Talin, M.D. Allendorf, Mof based electronic and opto-electronic devices, Chem. Soc. Rev. 43 (2014) 5994.

[3] (a) E.M. Miner, T. Fukushima, D. Sheberla, L. Sun, Y. Surendranath, M. Dincă, Electrochemical oxygen reduction catalysed by Ni_3(Hexaiminotriphenylene)$_2$, Nature Commun. 7 (2016) 10942.
(b) M.G. Campbell, D. Sheberla, S.F. Liu, T.M. Swager, M. Dincă, Cu_3(Hexaiminotriphenylene)$_2$: An electrically conductive 2D metal-organic framework for chemiresistive sensing, Angew. Chem. Int. Ed. 54 (2015) 4349.
(c) J. Park, M. Lee, D. Feng, Z. Huang, A.C. Hinckley, A. Yakovenko, X. Zou, Y. Cui, Z. Bao, Stabilization of hexaaminobenzene in a 2D conductive metal-organic framework for high power sodium storage, J. Am. Chem. Soc. 140 (2018) 10315.
(d) S. Roy, M. Das, A. Bandyopadhyay, S.K. Pati, P.P. Ray, T.K. Maji, Colossal increase in electric current and high rectification ratio in a photoconducting, self-cleaning, and luminescent schottky barrier nmof diode, J. Phys. Chem. C 121 (2017) 23803.
(e) S.S. Shinde, C.H. Lee, J.-Y. Jung, N.K. Wagh, S.-H. Kim, D.-H. Kim, C. Lin, S.U. Lee, J.-H. Lee, Unveiling Dual-Linkage 3D Hexaiminobenzene Metal-Organic Frameworks towards Long-Lasting Advanced Reversible Zn-Air Batteries. Energy Environ. Sci. 12 (2019) 727.
(f) D. Feng, T. Lei, M.R. Lukatskaya, J. Park, Z. Huang, M. Lee, L. Shaw, S. Chen, A.A. Yakovenko, A. Kulkarni, J. Xiao, K. Fredrickson, J.B. Tok, X. Zou, Y. Cui, Z. Bao, Robust and conductive two-dimensional metal-organic frameworks with exceptionally high volumetric and areal capacitance, Nat. Energy 3 (2018) 30.
(g) D. Sheberla, J.C. Bachman, J.S. Elias, C.-J. Sun, Y. Shao-Horn, M. Dinca, Conductive MOF electrodes for stable supercapacitors with high areal capacitance, Nat. Mater. 16 (2017) 220.
(h) X. Huang, S. Zhang, L. Liu, L. Yu, G. Chen, W. Xu, D. Zhu, Superconductivity in a copper(ii) based coordination polymer with perfect kagome structure, Angew. Chem. Int. Ed. 57 (2018) 146.

[4] (a) S. Takaishi, M. Hosoda, T. Kajiwara, H. Miyasaka, M. Yamashita, Y. Nakanishi, Y. Kitagawa, K. Yamaguchi, A. Kobayashi, H. Kitagawa, Electroconductive porous coordination polymer Cu[Cu(Pdt)$_2$] composed of donor and acceptor building units, Inorg. Chem. 48 (2009) 9048.
(b) Y. Kobayashi, B. Jacobs, M.D. Allendorf, J.R. Long, Conductivity, doping, and redox chemistry of a microporous dithiolene-based metal-organic framework, Chem. Mater. 22 (2010) 4120.

[5] (a) M.E. Ziebel, L.E. Darago, J.R. Long, Control of electronic structure and conductivity in two-dimensional metal-semiquinoid frameworks of titanium, vanadium, and chromium, J. Am. Chem. Soc. 140 (2018) 3040.
(b) S. Benmansour, A. Abhervé, P. Gómez-Claramunt, C. Vallés- García, C.J. Gómez-García, Nanosheets of two-dimensional magnetic and conducting Fe(II)/Fe(III) mixed-valence metal-organic frameworks, ACS Appl. Mater. Interfaces 9 (2017) 26210.
(c) J.A. DeGayner, I.-R. Jeon, L. Sun, M. Dincă, T.D. Harris, 2D conductive iron-quinoid magnets ordering up to T_c = 105 K via heterogenous redox chemistry, J. Am. Chem. Soc. 139 (2017) 4175.

[6] (a) M.-H. Zeng, Q.-X. Wang, Y.-X. Tan, S. Hu, H.-X. Zhao, L.-S. Long, M. Kurmoo, Rigid pillars and double walls in a porous metal-organic framework: Single-crystal to single-crystal, controlled uptake and release of iodine and electrical conductivity, J. Am. Chem. Soc. 132 (2010) 2561.
(b) X. Zhang, I. da Silva, R. Fazzi, A.M. Sheveleva, X. Han, B.F. Spencer, S.A. Sapchenko, F. Tuna, E.J.L. McInnes, M. Li, S. Yang, M. Schröder, Iodine adsorption in a redox-active metal-organic framework: electrical conductivity induced by host-guest charge-transfer, Inorg. Chem. 58 (2019) 14145.

[7] (a) A.A. Talin, A. Centrone, A.C. Ford, M.E. Foster, V. Stavila, P. Haney, R.A. Kinney, V. Szalai, F.E. Gabaly, H.P. Yoon, F. Léonard, M.D. Allendorf, Tunable electrical conductivity in metal-organic framework thin-film devices, Science 343 (2014) 66.
(b) C. Schneider, D. Ukaj, R. Koerver, A.A. Talin, G. Kieslich, S.P. Pujari, H. Zuilhof, J. Janek, M.D. Allendorf, R.A. Fischer, High electrical conductivity and high porosity in a Guest@MOF Material: Evidence of TCNQ Ordering within Cu_3BTC_2, Micropores. Chem. Sci. 9 (2018) 7405.

[8] J.G. Park, M.L. Aubrey, J. Oktawiec, K. Chakarawet, L.E. Darago, F. Grandjean, G.J. Long, J.R. Long, Charge delocalization and bulk electronic conductivity in the mixed- valence metal-organic framework Fe(1, 2, 3-Triazolate)$_2$(BF_4)$_x$, J. Am. Chem. Soc. 140 (2018) 8526.

[9] (a) L.S. Xie, G. Skorupskii, M. Dinca, Electrically conductive metal-organic frameworks, Chem. Rev. 120 (2020) 8536–8580.
(b) X. Kuang, S. Chen, L. Meng, J. Chen, X. Wu, G. Zhang, G. Zhong, T. Hu, Y. Li, C.-Z. Lu, Chem. Commun. 55 (2019) 1643–1646.

[10] (a) L. Sun, T. Miyakai, S. Seki, M. Dincă, Mn_2(2, 5-disulfhydrylbenzene-1, 4-dicarboxylate): A microporous metal-organic framework with infinite (-Mn-S-)∞ chains and high intrinsic charge mobility, J. Am. Chem. Soc. 135 (2013) 8185.
(b) F. Gándara, F.J. Uribe-Romo, D.K. Britt, H. Furukawa, L. Lei, R. Cheng, X. Duan, M. O'Keeffe, O.M. Yaghi, Porous, conductive metal-triazolates and their structural elucidation by the charge-flipping method, Chem. Eur. J. 18 (2012) 10595.

[11] L. Liu, J.A. DeGayner, L. Sun, D.Z. Zee, T.D. Harris, Reversible redox switching of magnetic order and electrical conductivity in a 2D manganese benzoquinoid framework, Chem. Sci. 10 (2019) 4652.

[12] (a) J.Y. Koo, Y. Yakiyama, G.R. Lee, J. Lee, H.C. Choi, Y. Morita, M. Kawano, Selective formation of conductive network by radical-induced oxidation, J. Am. Chem. Soc. 138 (2016) 1776.
(b) X. Kuang, S. Chen, L. Meng, J. Chen, X. Wu, G. Zhang, G. Zhong, T. Hu, Y. Li, C.-Z. Lu, Supramolecular aggregation of a redox-active copper-naphthalenediimide network with intrinsic electron conduction, Chem. Commun. 55 (2019) 1643.
(c) G. Haider, M. Usman, T.-P. Chen, P. Perumal, K.-L. Lu, Y.-F. Chen, Electrically driven white light emission from intrinsic metal-organic framework, ACS Nano 10 (2016) 8366.
(d) D. Chen, H. Xing, Z. Su, C. Wang, Electrical conductivity and electroluminescence of a new anthracene-based metal-organic framework with π-conjugated zigzag chains, Chem. Commun. 52 (2016) 2019.
(e) L. Qu, H. Iguchi, S. Takaishi, F. Habib, C.F. Leong, D.M. D'Alessandro, T. Yoshida, H. Abe, E. Nishibori, M. Yamashita, Porous molecular conductor: electrochemical fabrication of through-space conduction pathways among linear coordination polymers, J. Am. Chem. Soc. 141 (2019) 6802.

[13] S.S. Park, E.R. Hontz, L. Sun, C.H. Hendon, A. Walsh, T. Van Voorhis, M. Dincă, Cation-dependent intrinsic electrical conductivity in isostructural tetrathiafulvalene-based microporous metal-organic frameworks, J. Am. Chem. Soc. 137 (2015) 1774.

[14] P.I. Scheurle, A. Mähringer, A.C. Jakowetz, P. Hosseini, A.F. Richter, G. Wittstock, D.D. Medina, T. Bein, A highly crystalline anthracene-based MOF-74 series featuring electrical conductivity and luminescence, Nanoscale 11 (2019) 20949.

[15] J.K. Sun, Q. Xu, Functional materials derived from open framework templates/precusros: Synthesis and applications, Energy Environ. Sci. 7 (2014) 2071.

[16] (a) R. Das, P. Pachfule, R. Banerjee, P. Poddar, Metal and metal oxide nanoparticles synthesis from metal organic frameworks (MOFs): finding the border of metal and metal oxides, Nanoscale 4 (2012) 591.
(b) S. Singha, A. Saha, S. Goswami, S.K. Dey, S. Payra, S. Banerjee, S. Kumar, R. Saha, A metal organic framework to CuO nanospheres of uniform morphologyfor synthesis of α-aminonitriles under solvent-free conditions along with crystal structure of the MOF, Cry. Growth Des. 18 (2018) 189.
(c) S. Ekambaram, K.C. Patil, M. Maaza, Synthesis of lamp phosphors: facile combustion approach, J. Alloys Compd. 393 (2005) 81-92.
(d) B.T. Sone, E. Manikandan, A. Gurib-Fakim, M. Maaza, Sm_2o_3 nanoparticles green synthesis via callistemon viminalis' extract, J. Alloys Compd. 650 (2015) 357-362.
(e) S. Khamlich, E. Manikandan, B.D. Ngom, J. Sithole, O. Nemraoui, I. Zorkani, Synthesis, characterization, and growth mechanism of α-cr_2o_3 monodispersed particles, J. Phys. Chem. Solids. 72 (2011) 714-718.
(f) S. Karthik, P. Siva, K.S. Balu, R. Suriyaprabha, V. Rajendran, M. Maaza, Acalypha indica-mediated green synthesis of ZnO nanostructures under differential thermal treatment: effect on textile coating, hydrophobicity, uv resistance, and antibacterial, Adv. Powder Technol. 28 (2017) 3184-3194.

(g) N. Mayedwa, N. Mongwaketsi, S. Khamlich, K. Kaviyarasu, N. Matinise, Green synthesis of nickel oxide, palladium and palladium oxide synthesized via aspalathus linearis natural extracts: physical properties & mechanism of formation, Appl Surf Sci. 446 (2018) 266-272.
(h) H. Guo, T.T. Li, W.W. Chen, L.X. Liu, J.L. Qiao, J. Zhang, Self-assembly formation of hollow Ni-Fe-O nanocage architectures by metal–organic frameworks with high-performance lithium storage, Sci. Rep. 5 (2015) 13310, 5.
(i) H.B. Wu, B.Y. Xia, L. Yu, X.-Y. Yu, X.W. Lou, Porous molybdenum carbide nano-octahedrons synthesized via confined carburization in metal–organic frameworks for efficient hydrogen production, Nature Comm. 6 (2015) 6512, 1.
(j) P. Panchfule, X. Yang, Q. Zhu, N. Tsumori, T. Uchida, Q. Xu, From Ru nanoparticle-encapsulated metal–organic frameworks to highly catalytically active Cu/Ru nanoparticles-embedded porous carbon, J. Mater. Chem. A 5 (2017) 4835.
(k) Z. Liang, C. Qu, D. Xia, R. Zou, Q. Xu, Atomically dispersed metal sites in MOF-based materials for electrocatalytic and photocatalytic energy conversion, Angew. Chem. Int. Ed. 57 (2018) 9604.

[17] (a) R. Dai, W. Sun, Y. Wang, Ultrasmall tin nanodots embedded in nitrogen-doped mesoporous carbon: Metal-organic-framework derivation and electrochemical application as highly stable anode for lithium ion batteries, Electrochim. Acta 217 (2016) 123.
(b) A.C. Nwanya, D. Obi, K.I. Ozoemena, R.U. Osuji, C. Awada, A. Ruediger, M. Maaza, F. Rosei, F.I. Ezema, Facile synthesis of nanosheet-like CuO film and its potential application as a high-performance pseudocapacitor electrode, Electrochimica Acta 198 (2016) 220-230.
(c) B.T. Sone, A. Diallo, X.G. Fuku, A. Gurib-Fakim, M. Maaza, Biosynthesized CuO nano-platelets: physical properties & enhanced thermal conductivity nanofluidics, Arab. J. Chem. 13 (2020) 160-170.
(d) A.C. Nwanya, M.M. Ndipingwi, N. Mayedwa, L.C. Razanamahandry, C.O. Ikpo, Maize (zea mays l.) fresh husk mediated biosynthesis of copper oxides: potentials for pseudo capacitive energy storage, Electrochimica Acta 301 (2019) 436-448.

[18] H. Pang, B. Guan, W. Sun, Y. Wang, Metal-organic-frameworks derivation of mesoporous nio nanorod for high-performance lithium ion batteries, Electrochim. Acta. 213 (2016) 351.

[19] (a) J. Wu, Y. Song, R. Zhou, S. Chen, L. Zuo, H. Hou, L. Wang, Zn–Fe–ZIF-derived porous $ZnFe_2o_4$/C@NCNT nanocomposites as anodes for lithium-ion batteries, J. Mater. Chem. A. 3 (2015) 7793.
(b) W.J. Meng, W. Chen, L. Zhao, Y. Huang, M.S. Zhu, Y. Huang, Y.Q. Fu, F.X. Geng, J. Yu, X.F. Chen, Porous Fe_3O_4/carbon composite electrode material prepared from metal–organic framework template and effect of temperature on its capacitance, Nano Energy 8 (2014) 133.

[20] C.F. Lee, Y.C. Liu, S.S. Badsara, Transition-metal-catalyzed C-S bond coupling reaction, Chem. Asian J. 9 (2014) 706.

[21] (a) S.F. Nielsen, E.O. Nielsen, G.M. Olsen, T. Liljefors, D. Peters, Novel potent ligands for the central nicotinic acetylcholine receptor: Synthesis, receptor binding, and 3D-QSAR analysis, J. Med. Chem. 43 (2000) 2217.
(b) G. De Martino, M.C. Edler, G. La Regina, A. Cosuccia, M.C. Barbera, D. Barrow, R.I. Nicholson, G. Chiosis, A. Brancale, E. Hamel, M. Artico, R. Silvestri, New arylthioindoles: potent inhibitors of tubulin polymerization. 2. structure-activity relationships and molecular modeling studies, J. Med. Chem. 49 (2006) 947.

[22] (a) S.V. Ley, A.W. Thomas, Modern synthetic methods for copper-mediated C(aryl)-O, C(aryl)-N, and C(aryl)-S Bond Formation, Angew. Chem. Int. Ed. 43 (2003) 5400.
(b) C. Sambiagio, S.P. Marsden, A.J. Blacker, P.C. McGowan, Chem. Soc. Rev. 43 (2014) 3525-3550.

[23] T. Punniyamurthy, L. Rout, Recent advances in copper-catalyzed oxidation of organic compounds, Coord. Chem. Rev. 252 (2008) 134.

[24] (a) K.E. Torraca, X. Huang, C.A. Parrish, S.L. Buchwald, An efficient intermolecular palladium-catalyzed synthesis of aryl ethers, J. Am. Chem. Soc. 123 (2001) 10770.
(b) J. Mondal, A. Modak, A. Dutta, A. Bhaumik, Facile C–S coupling reaction of aryl iodide and thiophenol catalyzed by cu-grafted furfural functionalized mesoporous organosilica, Dalton Trans. 40 (2011) 5228.
(c) G.B.B. Varadwaj, S. Rana, K.M. Parida, Stable amine functionalized montmorillonite supported Cu, Ni catalyst showing synergistic and cooperative effectiveness towards C-S coupling reactions, RSC Adv. 3 (2013) 7570.
(d) E. Sperotto, G.P.M. van Klink, J.G. de Vries, G. van Koten, Ligand-free copper-catalyzed C-S coupling of aryl iodides and thiols, J. Org. Chem. 73 (2008) 5625.

[25] (a) G.T. Venkanna, H.D. Arman, Z.J. Tonzetich, Catalytic C-S cross-coupling reactions employing Ni complexes of pyrrole-based pincer ligands, ACS Catal. 4 (2014) 2941.
(b) X. Xu, J. Liu, J.J. Zhang, Y.W. Wang, Y. Peng, Nickel-mediated inter- and intramolecular C-S coupling of thiols and thioacetates with aryl iodides at room temperature, Org. Lett. 15 (2013) 3, 550.
(c) O. Bistri, A. Correa, C. Bolm, Iron-catalyzed C-O cross-couplings of phenols with aryl iodides, Angew. Chem. Int. Ed. 47 (2008) 586.

[26] S. Mandal, M. Mukherjee, S. Hazra, Evolution of electronic structures of polar phthalocyanine substrate interfaces, ACS Appl. Mater. Interfaces 12 (2020) 45564–45573.

[27] Bruker, APEX2, SAINT and SADABS, BRUKER AXS, Inc., Madison, Wisconsin, USA, 2008.

[28] G.M. Sheldrick, Crytal structure refinement with SHELX, Acta Cryst. C71 (2015) 3–8.

[29] L.J. Farrugia, Wingx and ORTEP for windows, an update, J. Appl. Crystallogr. 45 (2012) 849–854.

[30] A.L. Spek, Structure validation in chemical crystallography, Acta Cryst. D65 (2009) 148–155.

[31] L.J. Farrugia, ORTEP-3 for windows - a version of ORTEP-III with a graphical user interface (GUI), J. Appl. Crystallogr. 30 (1997) 565.

[32] X. He, C. Lu, D. Yuan, L. Chen, Q. Zhang, C. Wu, Hydrothermal synthesis, crystal structures, and properties of a class of 2D coordination polymers, Eur. J. Inorg. Chem. (2005) 4598.

[33] (a) R. Kitaura, K. Seki, G. Akiyama, S. Kitagawa, Porous coordination-polymer crystals with gated channels specific for supercritical gases, Angew. Chem. Int. Ed. 42 (2003) 428.
(b) J. Zhang, S. Kitagawa, Supramolecular isomerism, framework flexibility, unsaturated metal center, and porous property of Ag(I)/Cu(I) 3, 3', 5, 5'-tetrametyl-4, 4'-bipyrazolate, J. Am. Chem. Soc. 130 (2008) 907.

[34] T.K. Maji, M. Ohba, S. Kitagawa, Transformation from a 2D stacked layer to 3D interpenetrated framework by changing the spacer functionality: Synthesis, structure, adsorption, and magnetic properties, Inorg. Chem. 44 (2005) 9225.

[35] M.C. Biesinger, Advanced analysis of copper X-ray photoelectron spectra, Surf. Interface Anal. 49 (2017) 1325–1334.

[36] (a) X. Lv, W. Bao, J. Org. Chem. 72 (2007) 3863.
(b) D. Ma, Q. Cai, N, N-dimethyl glycine-promoted ullmann coupling reaction of phenols and aryl halides, Org. Lett. 5 (2003) 3799.
(c) H.-J. Cristau, P.P. Cellier, S. Hamada, J.-F. Spindler, M. Taillefer, A general and mild ullmann-type synthesis of diaryl ethers, Org. Lett. 6 (2004) 913.
(d) S. Jammi, S. Sakthivel, L. Rout, T. Mukherjee, S. Mandal, R. Mitra, P. Saha, T. Punniyamurthi, Cuo nanoparticles catalyzed c-n, c-o and c-s cross coupling reaction: scope and mechanism, J. Org. Chem. 74 (2009) 1971-1976.

[37] A.R. Hajipour, F. Dordahan, F. Rafiee, M. Mahdavi, C–n cross-coupling reaction catalysed by efficient and reusable cuo/sio2 nanoparticles under ligand-free conditions, Appl. Organ. Chem. 28 (2014) 809–813.

[38] S. Sagadevan, P. Murugasen, Electrical properties of copper oxide nanoparticles, J. Nano Res. 30 (2015) 1.